

Thermal Einstein-de Haas Effect Induced by Chiral Phonons in Carbon Nanotubes

Raimu Akimoto¹, Hiroyasu Matsuura², and Takahiro Yamamoto^{1,3,*}

¹ Department of Physics, Tokyo University of Science, 1-3 Kagurazaka, Shinjuku, Tokyo 162-8601, Japan

² National Institute of Advanced Industrial Science and Technology (AIST), Tsukuba 305-8568, Ibaraki, Japan

³ RIST, Tokyo University of Science, 1-3 Kagurazaka Shinjuku, Tokyo 162-8601, Japan

We investigate the effects of chirality on phonon thermal transport in semiconducting chiral single-walled carbon nanotubes (SWCNTs) using lattice dynamics combined with Boltzmann transport theory. We find that transverse acoustic and optical phonon modes, which are degenerate in nonchiral zigzag and armchair SWCNTs, are split in chiral SWCNTs, giving rise to finite phonon angular momentum associated with circular motion of individual atoms. This angular momentum is most efficiently generated in small-diameter nanotubes with intermediate chiral angles. Consequently, chiral SWCNTs are predicted to undergo thermally induced rigid-body rotation with an experimentally observable angular velocity via the thermal Einstein-de Haas effect.

The search for phenomena related to chirality has been actively pursued in various research fields, including the dynamics of chiral magnets,¹⁾ nano-optics,²⁾ and transport phenomena such as chiral-induced spin selectivity.^{3,4)} In particular, lattice dynamics in chiral crystals have recently attracted considerable attention, as phonons in chiral crystals can exhibit unconventional motions in which atomic nuclei undergo rotational motion, leading to finite phonon angular momentum.⁵⁻¹⁷⁾ Such phonon modes are referred to as chiral phonons and have been experimentally observed in a variety of materials, including α -HgS,⁸⁾ α -quartz,^{9,10)} and other chiral crystals.^{11,12)} From the theoretical perspective, chiral phonons have been extensively studied using both first-principles calculations¹³⁾ and model analyses.¹⁴⁾ Moreover, it has been proposed based on both experimental and theoretical studies that the angular momentum carried by chiral phonons can be transferred to the spin angular momentum of electrons,¹⁶⁾ highlighting chiral phonons as a promising concept in the context of spintronics. Furthermore, theoretical studies have suggested that applying a temperature gradient to a chiral crystal can induce macroscopic rotation of the crystal as a consequence of angular momentum conservation.^{9,13,15)} This phenomenon is analogous to the Einstein-de Haas (EdH) effect, in which a system undergoes mechanical rotation in response to magnetization,¹⁸⁾ and is therefore referred to as the thermal EdH effect.^{9,13,15)} Despite extensive theoretical interest, however, the thermal EdH effect has not yet been experimentally observed.

Carbon nanotubes (CNTs), which are experimentally realizable one-dimensional (1D) nanomaterials,¹⁹⁾ are broadly classified into three distinct structural types (zigzag, armchair, and chiral) depending on their rolling geometry.^{20,21)} The former two types, namely zigzag and armchair CNTs, are achiral and possess mirror symmetry with respect to the tube axis, with their nomenclature reflecting the characteristic atomic arrangements at the tube edge. The phonon properties of these achiral CNTs have been extensively investigated both theoretically and experimentally.²²⁻²⁸⁾ In contrast, chiral CNTs lack such symmetry and are intrinsically nonsymmetric. They exhibit handedness and are therefore not superimposable on their mirror images. As a consequence of this

structural asymmetry, chiral CNTs are expected to host intrinsic chiral phonons and to exhibit thermally induced EdH effects.

In this Letter, we present a comprehensive theoretical study of phonon angular momentum in semiconducting chiral single-walled carbon nanotubes (SWCNTs), focusing on the dependence of thermally induced phonon angular momentum on the tube diameter and chiral angle within the framework of the Boltzmann transport equation. Furthermore, we estimate the angular velocity of chiral SWCNTs under a temperature gradient arising from the thermally induced EdH effect.

First, we briefly describe a general formulation for calculating phonon angular momentum^{5,9,13,15)} and for quantifying the thermally induced EdH effect. For band insulators, where the charge and spin degrees of freedom of electrons can be neglected, the total angular momentum of the system under a temperature gradient can be expressed solely in terms of atomic degrees of freedom as

$$\mathbf{L}_{\text{tot}} = \mathbf{L}_{\text{lat}} + \mathbf{L}_{\text{ph}}, \quad (1)$$

where \mathbf{L}_{lat} denotes the angular momentum associated with rigid-body motion, and \mathbf{L}_{ph} is the angular momentum carried by phonons. The phonon angular momentum \mathbf{L}_{ph} is given by^{5,9,15)}

$$\mathbf{L}_{\text{ph}} = \sum_{\mathbf{q}, \lambda} \mathbf{l}_{\mathbf{q}, \lambda} \left\{ n(\omega_{\mathbf{q}, \lambda}) + \frac{1}{2} \right\}, \quad (2)$$

where $n(\omega_{\mathbf{q}, \lambda}) = n_0(\omega_{\mathbf{q}, \lambda}) + \delta n$, and $n_0(\omega_{\mathbf{q}, \lambda}) = 1/(e^{\hbar\omega_{\mathbf{q}, \lambda}/k_B T} - 1)$ is the Bose-Einstein distribution function for the phonon branch λ with wave vector \mathbf{q} at temperature T . Here, δn represents the deviation from equilibrium induced by the temperature gradient, and $\mathbf{l}_{\mathbf{q}, \lambda}$ is the angular momentum of a phonon mode characterized by \mathbf{q} and λ , defined as

$$\mathbf{l}_{\mathbf{q}, \lambda} = i\hbar \sum_j \mathbf{e}_{\mathbf{q}, j, \lambda} \times \mathbf{e}_{\mathbf{q}, j, \lambda}^*, \quad (3)$$

where $\mathbf{e}_{\mathbf{q}, j, \lambda}$ is the normalized displacement eigenvector of the phonon mode (\mathbf{q}, λ) corresponding to the j th atom in the unit cell. The phonon eigenvectors are obtained by solving the

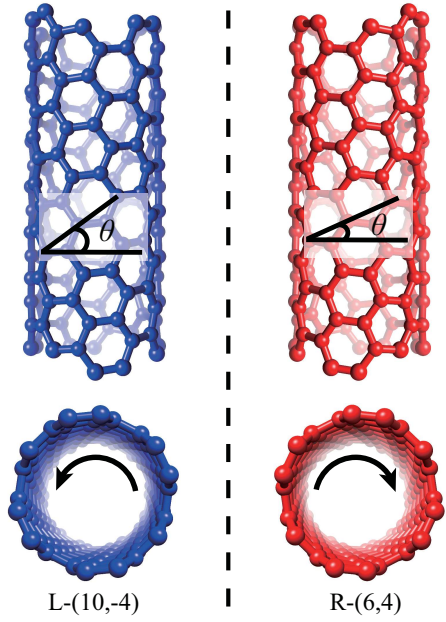


Fig. 1. (Color online) Illustrations of the unit-cell structures of left- (L-) and right-handed (R-) chiral (10,-4) and (6,4) SWCNTs, shown in blue and red, respectively. The chiral angle θ lies in the ranges $30^\circ < \theta < 60^\circ$ for L-handed structures and $0^\circ < \theta < 30^\circ$ for R-handed structures.

eigenvalue problem

$$\omega_{\mathbf{q},\lambda}^2 e_{\mathbf{q},\lambda}^\alpha - \sum_{j'} \sum_{\beta} D_{\alpha j}^{\beta j'}(\mathbf{q}) e_{\mathbf{q},j',\lambda}^\beta = 0, \quad (4)$$

where $D_{\alpha j}^{\beta j'}(\mathbf{q})$ is the dynamical matrix.

In equilibrium, the populations of two enantiomeric chiral phonons with wave vectors \mathbf{q} and $-\mathbf{q}$ are identical ($\delta n = 0$), resulting in a vanishing phonon angular momentum, $\mathbf{L}_{\text{ph}}^{\text{eq}} = 0$, where $\mathbf{L}_{\text{ph}}^{\text{eq}}$ denotes the phonon angular momentum in equilibrium. In contrast, when a temperature gradient is applied to the phonon system along the β direction, an imbalance between the populations of the two enantiomeric chiral phonons is induced ($\delta n \neq 0$), leading to a finite net phonon angular momentum $\Delta \mathbf{L}_{\text{ph}}^\alpha$.

In this situation, the nonequilibrium distribution δn can be described by the Boltzmann equation within the relaxation-time approximation as

$$\delta n = \frac{1}{T} \sum_{\beta} \hbar \omega_{\mathbf{q},\lambda} v_{\mathbf{q},\lambda}^\beta \tau_{\mathbf{q},\lambda} \left(-\frac{\partial n_0}{\partial \hbar \omega_{\mathbf{q},\lambda}} \right) (-\nabla_\beta T), \quad (5)$$

where $v_{\mathbf{q},\lambda}$ is the phonon group velocity and $\tau_{\mathbf{q},\lambda}$ is the phonon relaxation time. Substituting Eq. (5) into Eq. (2), the phonon angular momentum can be expressed as $\mathbf{L}_{\text{ph}}^\alpha = \mathbf{L}_{\text{ph}}^{\text{eq},\alpha} + \Delta \mathbf{L}_{\text{ph}}^\alpha$, where $\Delta \mathbf{L}_{\text{ph}}^\alpha$ is given by

$$\Delta \mathbf{L}_{\text{ph}}^\alpha = \frac{1}{T} \sum_{\beta} \sum_{\mathbf{q},\lambda} \hbar \omega_{\mathbf{q},\lambda} l_{\mathbf{q},\lambda}^\alpha v_{\mathbf{q},\lambda}^\beta \tau_{\mathbf{q},\lambda} \left(-\frac{\partial n_0}{\partial \hbar \omega_{\mathbf{q},\lambda}} \right) (-\nabla_\beta T). \quad (6)$$

Accordingly, the phonon angular momentum per unit volume induced by a temperature gradient along the β direction is defined as^{9,13,15}

$$J_{\text{ph}}^\alpha = \frac{\Delta \mathbf{L}_{\text{ph}}^\alpha}{V} \equiv \sum_{\beta} \kappa^{\alpha\beta} (-\nabla_\beta T), \quad (7)$$

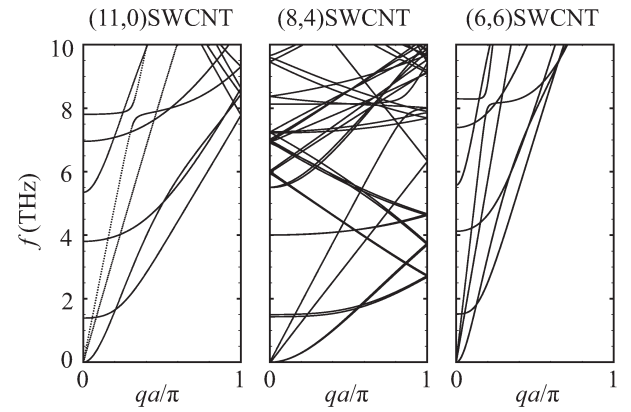


Fig. 2. Phonon dispersion relations of (11,0), (8,4), and (6,6) SWCNTs with unit-cell lengths $a = 0.43$, 1.15 , and 0.25 nm, respectively.

where V denotes the system volume and $\kappa^{\alpha\beta}$ is the thermal angular momentum coefficient, given by

$$\kappa^{\alpha\beta} = \frac{1}{VT} \sum_{\mathbf{q},\lambda} \hbar \omega_{\mathbf{q},\lambda} l_{\mathbf{q},\lambda}^\alpha v_{\mathbf{q},\lambda}^\beta \tau_{\mathbf{q},\lambda} \left(-\frac{\partial n_0}{\partial \hbar \omega_{\mathbf{q},\lambda}} \right). \quad (8)$$

Based on the conservation of total angular momentum described in Eq. (1), we obtain

$$\Delta \mathbf{L}_{\text{lat}}^\alpha = -\Delta \mathbf{L}_{\text{ph}}^\alpha. \quad (9)$$

This relation implies that the system undergoes rigid-body rotation about the α axis, which is referred to as the thermally induced EdH effect. By evaluating the thermal angular momentum coefficient $\kappa^{\alpha\beta}$ in Eq. (8), the angular momentum associated with rigid-body rotation, $\Delta \mathbf{L}_{\text{lat}}^\alpha$, can be quantitatively determined.

In this Letter, we focus on semiconducting chiral (n,m) SWCNTs with various tube diameters d_t and chiral angles θ . Figure 1 illustrates the left- (L-) and right-handed (R-) unit-cell structures of chiral (10,-4) and (6,4) SWCNTs. The chiral angle θ is defined as shown in Fig. 1; for L- and R-handed structures, θ lies in the ranges $30^\circ < \theta < 60^\circ$ and $0^\circ < \theta < 30^\circ$, respectively. The limiting cases $\theta = 0^\circ$ and 30° correspond to the highly symmetric zigzag and armchair SWCNTs, respectively.

We define the tube axis along the x direction and the system volume as $V = AL$, where L is the tube length and $A = \pi d_t^2$ is the effective cross-sectional area, with the tube thickness taken as $t = 3.4$ Å.^{29,30}

Figure 2 shows the phonon dispersion relations of (11,0), (8,4), and (6,6) SWCNTs. The phonon dispersions and eigenvectors are calculated from the dynamical matrix defined in Eq. (4) for optimized atomic structures. The interatomic forces between carbon atoms are modeled using the Tersoff potential,³¹ which is known to provide a reliable description of carbon–carbon interactions in SWCNTs. Among the four acoustic phonon modes in SWCNTs, the two modes exhibiting a quadratic dependence on the one-dimensional wave vector q correspond to the transverse acoustic (TA) phonon modes.²² As shown in Fig. 2, the TA phonon modes as well as some optical phonon modes are doubly degenerate in the highly symmetric zigzag and armchair SWCNTs.

Figure 3(a) shows the phonon angular momentum $l_{\mathbf{q},\lambda}^x$ for enantiomeric L- and R-handed structures of (10,-4) and (6,4)

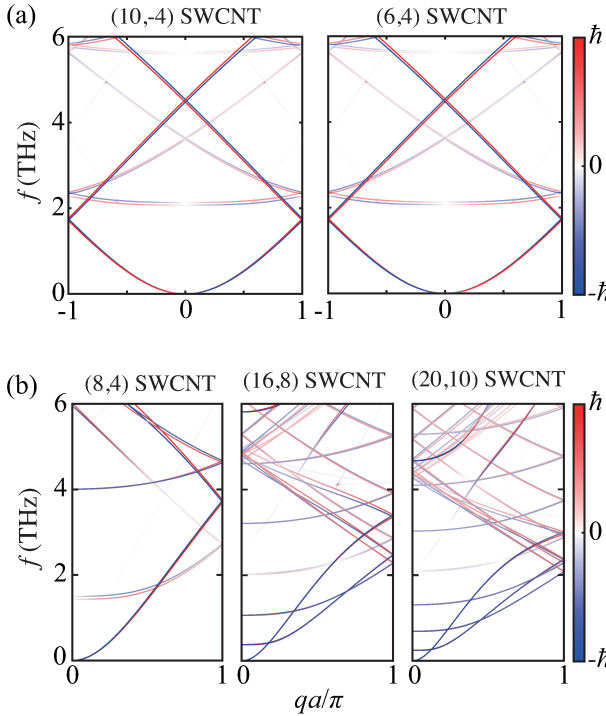


Fig. 3. (Color online) (a) Phonon angular momentum $l_{q,l}^x$ for (10,−4) and (6,4) SWCNTs with unit-cell length $a = 1.89$ nm. The blue and red colors represent the amplitudes of phonon angular momentum for left- and right-handed chiral phonon modes, respectively. (b) $l_{q,l}^x$ for (8,4), (16,8), and (20,10) SWCNTs with a fixed chiral angle $\theta = 19.1^\circ$ and unit-cell length $a = 1.14$ nm. The corresponding tube diameters are $d_t = 0.85, 1.68$, and 2.10 nm, respectively.

SWCNTs, calculated using Eq. (3). The blue and red colors represent the amplitudes of phonon angular momentum for L- and R-handed chiral phonon modes, respectively. In chiral SWCNTs, the TA phonon modes and certain optical phonon modes split into two branches carrying opposite signs of phonon angular momentum, as indicated by the red and blue colors. In addition, zone folding occurs at the Brillouin-zone boundary for these split branches, as shown in Fig. 3(a). These features are characteristic signatures of chiral SWCNTs. Furthermore, the L- and R-handed structures exhibit phonon angular momenta of opposite sign, reflecting their enantiomeric nature.

Figure 3(b) shows $l_{q,l}^x$ for R-handed (8,4), (16,8), and (20,10) SWCNTs at a fixed chiral angle $\theta = 19.1^\circ$, with corresponding tube diameters $d_t = 0.85, 1.68$, and 2.10 nm, respectively. With increasing d_t , the optical phonon modes shift toward lower frequencies. Focusing on relatively low-frequency chiral phonon modes, the splitting between the phonon branches is found to gradually decrease as d_t increases, indicating a tendency for the L- and R-handed chiral phonon branches to approach each other and eventually converge.

In this section, we discuss the dependence of the thermal angular momentum coefficient on the tube diameter d_t for chiral SWCNTs, focusing in particular on R-handed structures. From the symmetry of the SWCNT structure, $\kappa^{\alpha\beta}$ has finite values only in its diagonal components.¹³⁾ Furthermore, taking into account the one-dimensional nature of SWCNTs, we have $v_{q,l}^y = v_{q,l}^z = 0$, which implies that $\kappa^{yy} = \kappa^{zz} = 0$. There-

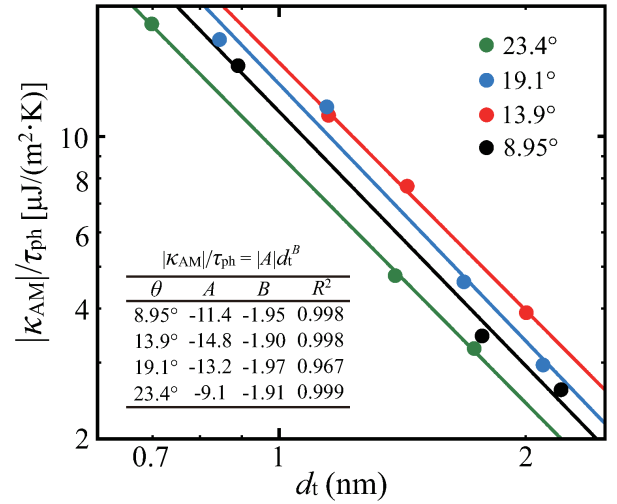


Fig. 4. (Color online) Dependence of $|\kappa_{AM}|/\tau_{ph}$ on the tube diameter d_t for chiral SWCNTs with four different chiral angles θ at 300 K. The corresponding values of θ are $8.95^\circ, 13.9^\circ, 19.1^\circ$, and 23.4° . The solid curves represent power-law fits of the form $|\kappa_{AM}|/\tau_{ph} = |A|d_t^B$, where A and B are fitting parameters.

fore, we focus on $\kappa^{xx} (\equiv \kappa_{AM})$. The coefficient κ_{AM} can be evaluated from Eq. (8) under a temperature gradient applied along the tube axis. The phonon relaxation time $\tau_{q,l}$ generally depends on phonon modes and frequencies and exhibits complex behavior in SWCNTs.^{29,32)} However, in order to clarify the dependences on d_t and the chiral angle θ in this Letter, we assume a constant phonon relaxation time τ_{ph} for simplicity.

Figure 4 shows the dependence of $|\kappa_{AM}|/\tau_{ph}$ on d_t for chiral SWCNTs with four different chiral angles θ at 300 K, namely $\theta = 8.95^\circ, 13.9^\circ, 19.1^\circ$, and 23.4° . The solid curves represent power-law fits of the form $|\kappa_{AM}|/\tau_{ph} = |A|d_t^B$, where A and B are the fitting parameters. The fitting parameters and the coefficient of determination for the overall fitted curves R^2 are summarized in the inset of Fig. 4. We find that $|\kappa_{AM}|/\tau_{ph}$ approximately follows a d_t^{-2} dependence for all values of θ . This result indicates that the generation of phonon angular momentum induced by chiral phonons is more efficient in SWCNTs with smaller diameters. This trend can be understood from the fact that the two transverse acoustic modes and the relevant optical modes approach each other as d_t increases, as shown in Fig. 3(b).

To examine the chiral-angle dependence of $|\kappa_{AM}|/\tau_{ph}$, we fix the tube diameter d_t and use the fitting parameters obtained in Fig. 4. Figure 5 shows the θ dependence of $|\kappa_{AM}|/\tau_{ph}$ for R-handed chiral SWCNTs with fixed diameters of $d_t = 1.2$ and 1.8 nm at 300 K. The red and blue curves correspond to sinusoidal fits of the form $|\kappa_{AM}|/\tau_{ph} = |C| \sin(D\theta)$, where the fitting parameters C and D are given in the inset of Fig. 5. We find that $|\kappa_{AM}|/\tau_{ph}$ reaches its maximum at $\theta = 15^\circ$, indicating that $|\kappa_{AM}|$ is maximized in chiral SWCNTs with strong helicity, corresponding to intermediate chiral angles between the zigzag ($\theta = 0^\circ$) and armchair ($\theta = 30^\circ$) limits.

Finally, we discuss the angular velocity of chiral SWCNTs under a temperature gradient based on the thermally induced EdH effect. The energy band gap of typical intrinsic semiconducting SWCNTs is approximately 1 eV; thus, thermal excitation of electrons is negligible at room temperature. Although

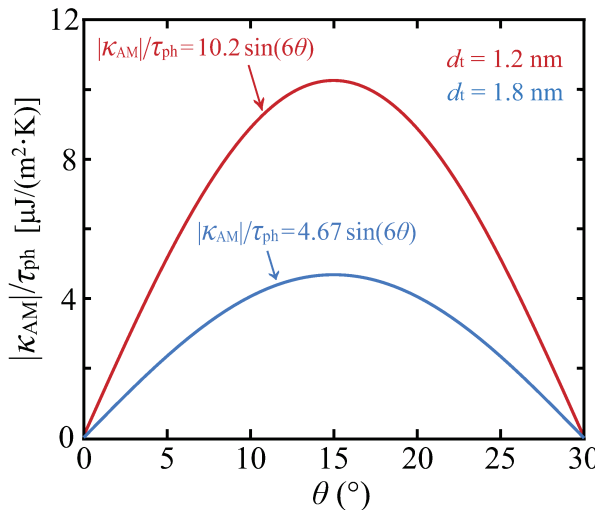


Fig. 5. (Color online) Dependence of $|\kappa_{\text{AM}}|/\tau_{\text{ph}}$ on the chiral angle θ for chiral SWCNTs at 300 K. The corresponding tube diameters are $d_t = 1.2$ and 1.8 nm. The red and blue curves represent sinusoidal fits of the form $|\kappa_{\text{AM}}|/\tau_{\text{ph}} = |C| \sin(D\theta)$, where C and D are fitting parameters. The fitting parameters (C, D) are $(-10.2, 6.0)$ and $(-4.67, 6.0)$, respectively.

electron-phonon interactions persist at this temperature, their impact on the spin-orbit interaction is considered minimal due to the strong covalent bonding of carbon atoms.³³⁾ Therefore, we assumed that the contribution of electron spin to the angular momentum is negligible. To estimate the angular velocity in this Letter, we treat a chiral SWCNT as a rigid body. As is well known from classical mechanics, the angular momentum associated with rigid-body rotation satisfies $J_{\text{ph}}^x V = -I\omega$,¹⁵⁾ in accordance with the conservation of total angular momentum described by Eq. (9). Here, $I = M\{(r - t/2)^2 + (r + t/2)^2\}/2$ is the moment of inertia, where M is the total mass of the nanotube and r is its radius. Accordingly, the angular velocity of rigid-body rotation in a chiral SWCNT is given by

$$\omega = \frac{-J_{\text{ph}}^x AL}{I}. \quad (10)$$

Using realistic parameters, $\nabla_x T = 10$ K, $\tau_{\text{ph}} = 10$ ps, and $L = 1.24 \mu\text{m}$, we estimate the angular velocity for a (6,5) SWCNT with $d_t = 0.76$ nm and $\theta = 27^\circ$. At 300 K, using $\kappa_{\text{AM}}/\tau_{\text{ph}} = -11.21 \mu\text{J}/(\text{m}^2 \cdot \text{K})$, we obtain $\omega \sim 1$ rad/s. This estimated angular velocity is significantly larger than previously reported values for chiral crystals.^{13,15)} The predicted large angular velocity is attributed to the repeated folding of phonon branches with high group velocities, including the TA mode, at the Brillouin zone boundaries. More fundamentally, the critical factor, which is intrinsically linked to the origin of this zone folding, is the relatively small moment of inertia of the SWCNT structure compared to that of other chiral crystals, resulting from its one-dimensional cylindrical geometry.

Conclusion

In this Letter, we have investigated the phonon angular momentum $I_{q\lambda}^x$ and the dependences of the thermal angular momentum coefficient κ_{AM} on the tube diameter d_t and chiral angle θ at 300 K for various semiconducting chiral SWCNTs. We have shown that the transverse acoustic modes and diameter-dependent optical phonon modes, which are degenerate in zigzag and armchair SWCNTs, split into two

branches in chiral SWCNTs. We find that κ_{AM} for chiral SWCNTs approximately scales as d_t^{-2} at a fixed chiral angle θ . In addition, $|\kappa_{\text{AM}}|$ exhibits a $\sin(6\theta)$ dependence at a fixed tube diameter, reaching its maximum at $\theta = 15^\circ$. Consequently, chiral SWCNTs with smaller diameters and intermediate chiral angles between the highly symmetric zigzag and armchair limits generate the largest phonon angular momentum. Furthermore, we have demonstrated that even a (6,5) SWCNT with $\theta = 27^\circ$, which is close to the armchair configuration, exhibits a larger angular velocity under a temperature gradient than previously studied chiral crystals. These results indicate that the thermally induced EdH effect in chiral SWCNTs is potentially observable in experiments.

Acknowledgments We are grateful to M. Ogata, T. Suenaga and A. Iida for the discussion. This work is supported by Grants-in-Aid for Scientific Research from the Japan Society for the Promotion of Science (No. 22KK0228 and No. 25K07199).

* takahiro@rs.tus.ac.jp

- 1) Y. Togawa, Y. Kousaka, K. Inoue, and J. Kishine, J. Phys. Soc. Jpn. **85**, 112001 (2016).
- 2) C. Kelly, D. A. MacLaren, K. McKay, A. McFarlane, A. S. Karimullah, N. Gadegaard, L. D. Barron, S. Franke-Arnold, F. Crimin, J. B. Götte, S. M. Barnett, and M. Kadodwala, Nat. Commun. **11**, 5169 (2020).
- 3) B. P. Bloom, Y. Paltiel, R. Naaman, and D. H. Waldeck, Chem. Rev. **2024**, 124, 1950-1991.
- 4) R. Naaman and D. H. Waldeck, J. Phys. Chem. Lett. **3**, 2178 (2012).
- 5) L. Zhang and Q. Niu, Phys. Rev. Lett. **112**, 085503 (2014).
- 6) L. Zhang and Q. Niu, Phys. Rev. Lett. **115**, 115502 (2015).
- 7) J. Kishine, A. S. Ovchinnikov, and A. A. Tereshchenko, Phys. Rev. Lett. **125**, 245302 (2020).
- 8) K. Ishito, H. Mao, Y. Kousaka, Y. Togawa, S. Iwasaki, T. Zhang, S. Murakami, J. Kishine, and T. Satoh, Nat. Phys. **19**, 35 (2023).
- 9) K. Ohe, H. Shishido, M. Kato, S. Utsumi, H. Matsuura, and Y. Togawa, Phys. Rev. Lett. **132**, 056302 (2024).
- 10) E. Oishi, Y. Fujii, and A. Koreeda, Phys. Rev. B **109**, 104306 (2024).
- 11) H. Ueda, M. García-Fernández, S. Agrestini, C. P. Romao, J. van den Brink, N. A. Spaldin, K.-J. Zhou, and U. Staub, Nature (London) **618**, 946 (2023).
- 12) K. Ishito, H. Mao, K. Kobayashi, Y. Kousaka, Y. Togawa, H. Kusunose, J. Kishine, and T. Satoh, Chirality **35**, 338 (2023).
- 13) M. Hamada, E. Minamitani, M. Hirayama, and S. Murakami, Phys. Rev. Lett. **121**, 175301 (2018).
- 14) H. Tsunetsugu and H. Kusunose, J. Phys. Soc. Jpn. **92**, 023601 (2023).
- 15) H. Chen, W. Wu, J. Zhu, Z. Yang, W. Gong, W. Gao, S. A. Yang, and L. Zhang, Nano Lett. **22**, 1688 (2022).
- 16) M. Matsuo, J. Ieda, E. Saitoh, and S. Maekawa, Phys. Rev. Lett. **106**, 076601 (2011).
- 17) H. Zhang, N. Peshcherenko, F. Yang, T. Z. Ward, P. Raghuvanshi, L. Lindsay, C. Felser, Y. Zhang, J.-Q. Yan, and H. Miao, Nat. Phys. **21**, 1387-1391 (2025).
- 18) A. Einstein and W. J. de Haas, Phys. Ges. **17**, 152 (1915).
- 19) S. Iijima and T. Ichihashi, Nature **363**, 603 (1993).
- 20) R. Saito, M. Fujita, G. Dresselhaus, and M. S. Dresselhaus, Appl. Phys. Lett. **60**, 2204 (1992).
- 21) J. W. Mintmire, D. H. Robertson, and C. T. White, J. Phys. Chem. Solids **54**, 1835 (1993).
- 22) H. Suzuura and T. Ando, Phys. Rev. B **65**, 235412 (2002).
- 23) R. Saito, T. Takeya, T. Kimura, G. Dresselhaus, and M. S. Dresselhaus, Phys. Rev. B **57**, 4145 (1998).
- 24) G. D. Mahan and G. S. Jeon, Phys. Rev. B **70**, 075405 (2004).
- 25) J. Wang and J.-S. Wang, J. Appl. Phys. **105**, 063509 (2009).
- 26) T. Yamamoto, S. Watanabe, and K. Watanabe, Phys. Rev. Lett. **92**, 075502 (2004).

- 27) T. Yamamoto, S. Konabe, J. Shiomi, and S. Maruyama, *Appl. Phys. Express* **2**, 095003 (2009).
- 28) T. Yamamoto and K. Watanabe, *Phys. Rev. Lett.* **96**, 255503 (2006).
- 29) Y. Gu and Y. Chen, *Phys. Rev. B* **76**, 134110 (2007).
- 30) E. Pop, D. Mann, Q. Wang, K. Goodson, and H. Dai, *Nano Lett.* **6**, 96 (2006).
- 31) L. Lindsay and D. A. Broido, *Phys. Rev. B* **81**, 205441 (2010).
- 32) J. X. Cao, X. H. Yan, Y. Xiao, J. W. Ding, *Phys. Rev. B* **69**, 073407 (2004).
- 33) T. Ando, *J. Phys. Soc. Jpn.* **69**, 1757 (2000).